Check for updates

Ag₃PO₄ electrocatalyst for oxygen reduction reaction: enhancement from positive charge†

Yong Qin,‡[a] Fan Li,‡[a] Peng Tu,‡[b] Yanling Ma,[a] Wenlong Chen,[a] Fenglei Shi,[a] Qian Xiang,[a] Hao Shan,[a] Lifu Zhang,[a] Peng Tao, [ID][a] Chengyi Song, [ID][a] Wen Shang,[a] Tao Deng, [ID][a] Hong Zhu*[abc] and Jianbo Wu [ID] *[ac]

We have demonstrated Ag₃PO₄ as an active non-Pt electrocatalyst with enhanced activity compared with Ag for oxygen reduction reaction (ORR). Density functional theory reveals that better ORR performance of Ag atoms on Ag₃PO₄ surface than that on pure silver surface originates from more appropriate oxygen adsorption on positively charged Ag atoms. Further study of the surface geometry of Ag₃PO₄ including tetrahedron, rhombic dodecahedron and cube indicates that the highest density of Ag and appropriate oxygen adsorption on {110} surface of rhombic dodecahedral Ag₃PO₄ lead to the highest ORR activity, which is about 12 times that of Pt catalysts from a commercial perspective. It may be applicable for developing low-cost and highly active non-Pt catalytic materials from a broader range of material systems.

Introduction

Oxygen reduction reaction (ORR) is one of the crucial limiting factors in commercialization of proton-exchange membrane fuel cells due to its sluggish kinetics.[1-5] Platinum group metal has been demonstrated to be the most practical ORR catalyst because of its appropriate adsorption of oxygen, which facilitates the adsorption of oxygen on Pt surface for reduction and the desorption of the intermediate OH for turnover.[6] In the past few years, great efforts have been made to design active ORR catalysts by shape control, composition engineering and modulation of element distribution.[7-16] However, Pt-based electrocatalysts are usually of high cost and from limited reserves, which bring limitations for the commercialization of these catalysts, especially for mass production of vehicles.[17] Thus, a large number of substitutes for Pt have been considered including metals (Pd, Fe, Co, Mn, *etc.*),[18,19] metal oxides,[20-22] carbon materials,[23] Fe–N–C,[24] and perovskites.[25,26]

Non-platinum monometallic catalysts such as Pd,[27,28] Au,[29-31] and Ag[32] are capable of catalyzing the ORR. However, most of these cannot resist the oxidative etching in the working condition of the ORR, including the electrolyte and high potential.[33,34] For example, Ag is the most abundant precious metal, which is 38 times that of Pt in terms of global reserves,[35] illustrating that Ag is much easier to obtain and use for mass production. However, the standard redox potential of Ag is 0.7993 V (ref. 36), which results in the oxidation and degradation of Ag-based catalysts at high potential under working conditions.

In this paper, we have demonstrated that the oxidized Ag⁺ ion in the lattice of Ag₃PO₄ can still electro-catalytically reduce oxygen, which makes Ag₃PO₄ nanoparticles a non-Pt ORR catalyst, and also avoid the aforementioned oxidation limitation. Moreover, Ag⁺ ions of Ag₃PO₄ are even more active than Ag atoms. Density functional theory calculation reveals that the positively charged Ag in the lattice of Ag₃PO₄ leads to a more appropriate oxygen adsorption, and therefore to enhanced ORR activity compared to pure Ag. Further study of the surface geometry of Ag₃PO₄ by altering Ag₃PO₄ nanoparticles from tetrahedron to rhombic dodecahedron and cube shows that the highest density of Ag and appropriate oxygen adsorption on {110} surface of rhombic dodecahedral Ag₃PO₄ lead to the improved ORR activity, which is about 12 times that of Pt catalysts from a commercial perspective.

Experimental section

Materials

Silver acetate (CH₃COOAg, 99.5%), sodium phosphate dibasic (Na₂HPO₄, 99.99%), potassium hydroxide (KOH, 99.99%) and short multi-walled carbon nanotubes (CNT) were purchased from Aladdin. Silver nitrate (AgNO₃, 99.8%) and ammonia solution (NH₃·H₂O) were purchased from Shanghai Ling Feng

[a] State Key Laboratory of Metal Matrix Composites, School of Materials Science and Engineering, Shanghai Jiao Tong University, 800 Dongchuan Road, Shanghai, 200240, People's Republic of China. E-mail: jianbowu@sjtu.edu.cn; hong.zhu@sjtu.edu.cn

[b] University of Michigan – Shanghai Jiao Tong University Joint Institute, Shanghai Jiao Tong University, 800 Dongchuan Road, Shanghai, 200240, P. R. China

[c] Materials Genome Initiative Center, Shanghai Jiao Tong University, 800 Dongchuan Road, Shanghai, 200240, P. R. China

† Electronic supplementary information (ESI) available. See DOI: 10.1039/c7ra12643c

‡ These authors contribute equally to this work.

Chemical Reagent Co. Ltd. Phosphoric acid (H_3PO_4, 85.0%) was purchased from Sinopharm Chemical Reagent Co. Ltd. Ethanol (CH_3CH_2OH, 99.7%) was purchased from Changshou City Yangyuan Chemical Co. Ltd. Carbon (C, Vulcan®XC-72R) purchased from Cabot was used as support material. Oxygen (O_2, 99.999%) and argon (Ar, 99.999%) were purchased from Shanghai Weichuang Standard Gas Analytical Technology Co. Ltd.

Synthesis of Ag_3PO_4 particles

Ag_3PO_4 particles were synthesized by a simple method.[37] For Ag_3PO_4 tetrahedron, 12 mmol $AgNO_3$ was dissolved in 80 ml ethanol with strong magnetic stirring. Meanwhile, 20 ml H_3PO_4 was blended with 80 ml ethanol under rapid magnetic stirring. After $AgNO_3$ was completely dissolved in ethanol solution and these two solutions were transparent, the $AgNO_3$-ethanol mixed solution was added to the H_3PO_4-ethanol solution drop by drop. Sediment appeared quickly and then disappeared under strong stirring. $AgNO_3$-ethanol mixture was added dropwise continuously until H_3PO_4-ethanol mixed solution became cloudy; at this moment, the whole H_3PO_4-ethanol and $AgNO_3$-ethanol suspension were added back to the $AgNO_3$-ethanol solution. There appeared a yellow precipitate immediately. After stirring for 1 hour, the mixed solution turned a bright green colour, indicating the nucleation and growth of Ag_3PO_4 with specific shapes. Finally, the product was washed with deionized water and ethanol three times each.[37]

For Ag_3PO_4 rhombic dodecahedron, 0.2 g CH_3COOAg was dissolved in 100 ml deionized water. And then an as-prepared Na_2HPO_4 solution (0.15 M) was added to the above solution dropwise. A golden yellow precipitate was formed. After 1 hour of stirring, the obtained products were washed with deionized water and ethanol three times to remove CH_3COO^-.

With regard to the Ag_3PO_4 cube, 0.2 g $AgNO_3$ was dissolved in 100 ml deionized water. Ammonia aqueous solution (0.1 M) was added drop by drop to the $AgNO_3$-water solution. When the above solution became transparent, an as-prepared Na_2HPO_4 solution (0.15 M) was added to the mixed solution. After stirring for 1 hour, the samples were washed with deionized water and ethanol to remove impurities.[38]

Finally, these three kinds of obtained samples were dried in the atmosphere, and it was ensured that all moisture was removed from the catalyst.

Material characterization

Scanning electron microscopy (SEM) micrographs were obtained using an LV UHR FE-SEM. The SEM was operated at an accelerating voltage of 5 kV. Transmission electron microscopy (TEM) images were obtained using a JEOL JEM-2100F microscope with an accelerating voltage 200 kV. X-ray diffraction (XRD) patterns were obtained using a Shimadzu LabX XRD-6100 X-ray diffractometer with Cu source. The XRD patterns were recorded from 10° to 90° with a scanning rate of 0.167° s^{-1}.

Preparation of catalyst

These three kinds of Ag_3PO_4 with different morphologies can be used as catalysts for the ORR. In order to improve the ORR performance, Ag_3PO_4 was mixed with carbon. Vulcan XC-72 carbon and CNT were chosen as the carbon support, becoming Ag_3PO_4/C and Ag_3PO_4/CNT catalysts. The carbon and CNT were each dissolved in methanol. After sonicating for 1 hour, Ag_3PO_4 with different facets were added. And the mass ratio of Ag_3PO_4 particles to carbon was 1 : 4. The mixture was stirred for at least 24 hours. Afterwards, the solid products were obtained by centrifugation. Subsequently, the samples were dried by freeze-drying for ORR tests.

Electrochemical measurements

A three-electrode cell was used to test the electrochemical performance. A glassy-carbon rotating disk electrode (RDE), whose area was 0.196 cm^2, was used as the working electrode. The counter electrode was a 5 cm platinum wire. And a reversible hydrogen electrode (RHE) was used as the reference, which was put in a separate compartment connected with the main cell through a salt bridge. The electrolyte for Ag_3PO_4-related ORR tests was 0.1 M KOH. In order to prepare a catalyst for the working electrode, 5 mg of Ag_3PO_4, Ag_3PO_4/C and Ag_3PO_4/CNT were dissolved in 5 ml solution, which was composed of 4 ml deionized water, 1 ml isopropanol and 25 μl Nafion (5%). The mixed solution was sonicated for 15 min, forming a uniform ink. So as to ensure the mass of Ag_3PO_4 used for the catalyst was constant, we selected 10 μl solutions in pure Ag_3PO_4 ink. Meanwhile, it is necessary to select 50 μl solutions in Ag_3PO_4/C and Ag_3PO_4/CNT ink. This ink was added to the RDE and dried under a warm flow of air. The Pt/C and Ag were designed as 40.82 g cm^{-2} and 40.82 g cm^{-2} on the RDE by following a similar procedure. The electrochemical active surface area was obtained from cyclic voltammetry curves, which were measured at room temperature in argon-saturated 0.1 M KOH solution. The potential scan rate was 50 mV s^{-1}. And then the ORR properties were tested in 0.1 M KOH solution that was pumped with oxygen for 30 min in advance. The scan rate for ORR measurements was 10 mV s^{-1}.

Results and discussion

Fig. 1a shows a typical SEM micrograph of the as-synthesized Ag_3PO_4 tetrahedrons. It can be seen that single crystalline Ag_3PO_4 tetrahedrons with smooth surfaces have been fabricated in large quantities. The average edge length of the Ag_3PO_4 tetrahedrons is 1140 nm (Fig. S2a†). The as-prepared Ag_3PO_4 tetrahedron was enclosed completely by four well-defined {111} planes (Fig. 1a and S1a†). Fig. 1b shows a representative SEM image of the Ag_3PO_4 rhombic dodecahedrons, and the average edge length of these is 478.2 nm with regular rhombic dodecahedral morphology. Furthermore, the SEM and TEM micrographs (Fig. S1b†) indicate that the Ag_3PO_4 rhombic dodecahedron was enclosed completely by twelve {110} facets. Interestingly, when using $[Ag(NH_3)_2]^+$ complex replacing silver acetate in this synthetic system, we can obtain uniform Ag_3PO_4 cubes (Fig. 1c). In addition, the enlarged SEM and TEM (Fig. S1c†) micrographs indicate that the as-prepared Ag_3PO_4 cube was enclosed by six square {100} planes, whose average
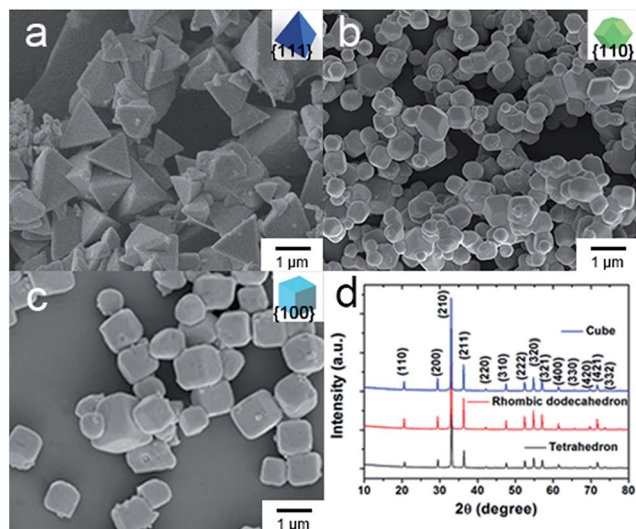
Fig. 1 SEM micrographs of Ag_3PO_4 crystals: (a) tetrahedron, (b) rhombic dodecahedron, (c) cube. (d) XRD patterns of faceted Ag_3PO_4 crystals.

edge length is 676.7 nm. Moreover, the XRD patterns (Fig. 1d) clearly show that all of the diffraction peaks of the tetrahedral, rhombic dodecahedral and cubic particles could be indexed to that of body-centered cubic crystalline Ag_3PO_4 (JCPDS no. 06-0505). And there are no other impurity peaks or trace peaks associated with the precursors found in the patterns of as-synthesized samples.

The catalytic performance of the three Ag_3PO_4/C catalysts towards the ORR was investigated using the three-electrode method (Fig. 2a–c). The polarization curves of the tetrahedron and rhombic dodecahedron have positive shifts of 5 mV and 30 mV compared with that of the cube. The corresponding ORR

Fig. 2 ORR polarization curves of tetrahedral, rhombic dodecahedral and cubic Ag_3PO_4 catalysts: (a) pure Ag_3PO_4, (b) Ag_3PO_4 and carbon, (c) Ag_3PO_4 and CNT. The mass of Ag_3PO_4 is 10 μg. (d) Comparison of the mass current density based on 0.8 V (vs. RHE), ORR properties, of cubic, rhombic dodecahedral and tetrahedral Ag_3PO_4.

mass activity (i_m) of tetrahedral, rhombic dodecahedral and cubic Ag_3PO_4 is 4.65 mA mg_{Ag}^{-1}, 5.57 mA mg_{Ag}^{-1} and 3.49 mA mg_{Ag}^{-1}, respectively. The mass activities are obtained from the following equation:

$$\frac{1}{i_k} = \frac{1}{i_{disk}} - \frac{1}{i_d}$$ (1)

where i_k is the kinetic current density, i_{disk} is the measured current density, which is got at 0.8 V, and i_d is the diffusion-limiting current density. Then

$$i_m = \frac{i_k \times S}{m} \times \frac{1}{77.3\%}$$ (2)

where S is the area of loading catalysts, m is the loading mass of Ag_3PO_4, and the value "77.3%" means the relative molecular mass ratio of Ag in Ag_3PO_4 crystal.

When Ag_3PO_4 is mixed with carbon, the corresponding ORR performances of all Ag_3PO_4 particles show great improvement, which is 193% for the tetrahedron, 201% for the rhombic dodecahedron, and 216% for the cube. The ORR performance is further boosted when Ag_3PO_4 is combined with CNT, for which the improvement is 256% for the tetrahedron, 220% for the rhombic dodecahedron, and 271% for the cube.

From Fig. S3,† we can find that the Ag_3PO_4 crystals were completely dispersed in carbon and CNT. Carbon material such as Vulcan XC-72 and CNT is not only a silver phosphate crystal support, but also plays a role of collaborative catalyst.[39] The incorporation of carbon can increase the electrochemical accessible surface areas and electron conductivity.[40] And CNT was discovered as a promising support material, due to its specific surface area, electrical conductivity and electrochemical stability.[41–43] So the dramatic improvements of catalytic activity are because Ag_3PO_4 with CNT has better electrical conductivity and greater specific surface area than Ag_3PO_4 and Ag_3PO_4 with carbon.

Indeed, the rhombic dodecahedral Ag_3PO_4/CNT exhibits a mass activity of 13.76 mA $mg_{Ag_3PO_4}^{-1}$ (0.0178 mA $μg_{Ag}^{-1}$), which is about 12% of that of a commercial Pt/C catalyst (0.1495 mA $μg_{Pt}^{-1}$; Fig. S10†). This result of Pt/C is similar to reported data.[44] In fact, considering that the price of Ag is only 1/100 of that of Pt,[45,46] the rhombic dodecahedral Ag_3PO_4/CNT catalyst is about 12 times as active as Pt catalysts from a commercial perspective. Moreover, the global reserve of Pt metal is about 38 times less than that of Ag, illustrating that Ag is much easier to acquire and use for mass production.

The long-term stability of the catalysts was evaluated through accelerated durability tests (Fig. S7 and S8†). The mass activity of rhombic dodecahedral Ag_3PO_4/CNT shows 12.5% loss after 5000 cycles, while the reported loss for Pt/C catalyst was 31.3% after 5000 cycles.[47] Therefore, the rhombic dodecahedral Ag_3PO_4/CNT catalyst shows better durability than commercial Pt/C.

The ORR performance of the Ag_3PO_4/C catalysts was further examined as a function of the rotation speed of RDE from 400 to 2500 rpm (Fig. 3a–c). Fig. 3d shows the Koutecky–Levich plots as a function of potential for Ag_3PO_4/C catalysts bounded with each of {111}, {110} and {100}, which shows different slopes,
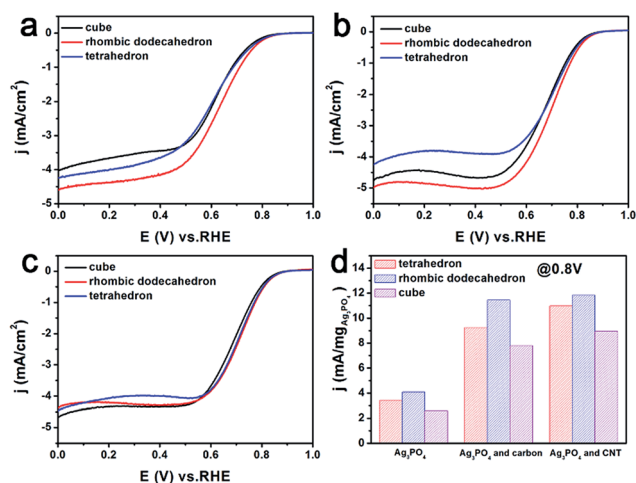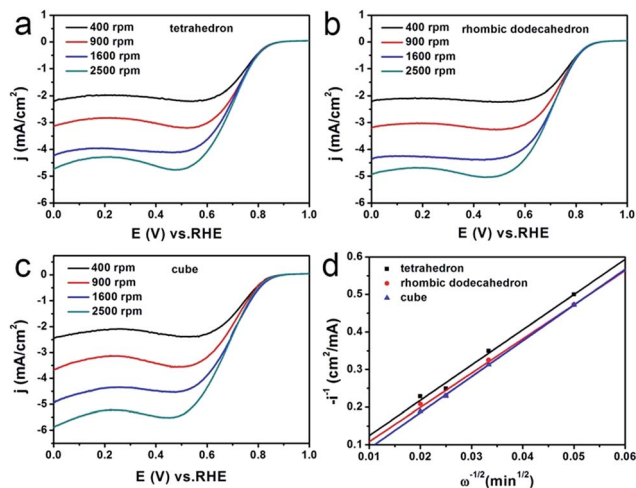
Fig. 3 RDE voltammograms for the ORR of (a) tetrahedral, (b) rhombic dodecahedral and (c) cubic Ag_3PO_4/C electrocatalysts at various rotation rates. (d) Koutecky–Levich plots of the rotating disk current at 0.3 V (vs. RHE). The tests were conducted in O_2-saturated 0.1 M KOH solution and the scan rate was kept at 10 mV s^{-1}.

Fig. 4 (a) The crystal structure of Ag_3PO_4. Illustration that the favored adsorption site on (b) the {111} planes of Ag_3PO_4 crystals is Ag-top site with $E_{ads} = -2.151$ eV, (c) the {110} planes of Ag_3PO_4 crystals is Ag-top site with $E_{ads} = -0.83$ eV, and (d) the {100} planes of Ag_3PO_4 crystals is Ag–P bridge with $E_{ads} = -2.996$ eV. (e) Volcano plot of pure Ag and different surfaces of Ag_3PO_4. E_{ads} is the adsorption energy of oxygen.

indicating the different reaction kinetics occurring on the three faceted Ag_3PO_4/C catalysts. The number of transferred electrons during the ORR has also been investigated via changing the rotation speed of the RDE ranging from 400 to 2500 rpm (Fig. 3a–c).

Then, we calculated the slopes of the three Koutecky–Levich plots from the following equation:

$$\frac{1}{i_{disk}} = \frac{1}{i_k} + \frac{1}{i_d} = \frac{1}{i_k} + \frac{1}{B\omega^{\frac{1}{2}}} \quad (3)$$

where i_k is the kinetic current density, i_{disk} is the measured current density, and i_d is the diffusion-limiting current density. B is the Levich constant and ω is the rotation rate of the electrode. B can be directly acquired from the slope of the Koutecky–Levich plot (Fig. 3d).

The relationship between the Levich constant B and the number of transferred electrons n during ORR could be obtained as follows:

$$B = 0.2nFD_0^{2/3}C_0\nu^{-1/6} = 3.5 \times 10^{-5}n \quad (4)$$

in this equation, n represents the number of electrons transferred, F refers to the Faraday constant, D_0 is the diffusion coefficient of oxygen gas (1.9×10^{-5} cm^2 s^{-1}), C_0 represents the concentration of oxygen gas in aqueous solution (1.1×10^{-5} mol cm^{-3}), and ν is the kinematic viscosity of water (0.01 cm^2 s^{-1}).[44]

Therefore, from the slopes of the three curves shown in Fig. 3d, we can obtain the value of n, which is 3.1, 3.2, and 3.0, respectively, for the tetrahedral, the rhombic dodecahedral, and the cubic Ag_3PO_4/C catalysts. This indicates that the reduction from O_2 to OH^- on these Ag_3PO_4/C catalysts can be regarded as mixed pathways of four-electron and two-electron processes. But the {110} of Ag_3PO_4 shows a higher portion of the four-electron pathway than the other two facets.
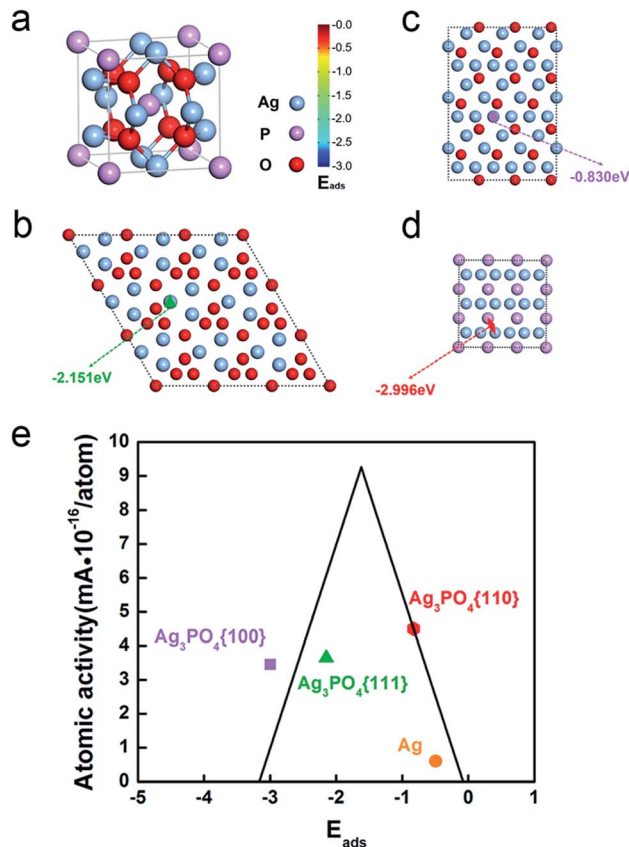
Fig. 4a shows the crystal structure of Ag_3PO_4 which possesses a body-centered cubic structure. Fig. 4b–d shows the surface atomic configuration of the {111}, {110}, and {100} close-packed planes of Ag_3PO_4 crystals. Obviously, all the facets including {111}, {110} and {100} have different terminations composed of Ag atoms, O atoms or P atoms. However, the outermost Ag atomic ratio, that is the Ag atomic ratio involved in the reaction, and its atomic activity (Table S2†) are different on the three surfaces (Table S2,† see the calculation details in ESI†).

We calculated the adsorption of oxygen at various sites on these three surfaces (Table S4†). The most stable oxygen adsorption energies, E_{ads}, on different faceted Ag_3PO_4 are shown in Fig. 4, namely, −2.151 eV, −0.830 eV and −2.996 eV for {111}, {110} and {100} facets, respectively (Table S4†). The rhombic dodecahedral Ag_3PO_4 with {110} planes shows the best ORR performance of the three different morphologies of Ag_3PO_4 because of the appropriate adsorption energy of oxygen based on the Sabatier principle (the volcano plot in Fig. 4e).[48]

Moreover, the Ag atoms in the lattice of Ag_3PO_4 also show a better atomic ORR performance than Ag atoms in pure silver. If only counting the surface Ag atoms participating in the ORR, Ag of Ag_3PO_4 (4.50425×10^{-16} mA per atom$_{Ag}$ for Ag_3PO_4{110})

is 7.5 times better than pure Ag (5.99961×10^{-17} mA per atom$_{Ag}$) (Table S3†). Based on the calculation, the Ag atoms on Ag$_3$PO$_4$ have a stronger binding with oxygen than pure Ag (-0.49 eV in Fig. 4e and Table S5†) due to the positive charge on Ag of Ag$_3$PO$_4$, which leads to a downshift of density of states of Ag, and hence the 7.5 times enhancement of ORR activity.[48]

Conclusions

In summary, we have demonstrated Ag$_3$PO$_4$ nanoparticles as an active non-Pt ORR catalyst. The Ag$^+$ ions in the lattice of Ag$_3$PO$_4$ show very good ORR performance compared with the Ag atoms of pure Ag due to more appropriate oxygen adsorption on positively charged Ag atoms. Among the three geometric structures of Ag$_3$PO$_4$, namely tetrahedron, rhombic dodecahedron, and cube, the highest density of Ag atoms and appropriate oxygen adsorption on {110} surface of rhombic dodecahedral Ag$_3$PO$_4$ lead to the highest ORR activity, which is about 12 times that of Pt catalysts from a commercial perspective. This fundamental discovery may be applicable for developing low-cost and highly active non-Pt catalytic materials. This demonstration provides an alternative strategy to develop low-cost and highly active non-Pt catalytic materials from a broader range of material candidates.

Conflicts of interest

There are no conflicts to declare.

Acknowledgements

Notes and references

1 M. K. Debe, *Nature*, 2012, **486**, 43–51.
2 H. A. Gasteiger, S. S. Kocha, B. Sompalli and F. T. Wagner, *Appl. Catal., B*, 2005, **56**, 9–35.
3 F. T. Wagner, B. Lakshmanan and M. F. Mathias, *J. Phys. Chem. Lett.*, 2010, **1**, 2204–2219.
4 M. H. Shao, Q. W. Chang, J. P. Dodelet and R. Chenitz, *Chem. Rev.*, 2016, **116**, 3594–3657.
5 A. A. Gewirth and M. S. Thorum, *Inorg. Chem.*, 2010, **49**, 3557–3566.
6 J. B. Wu and H. Yang, *Acc. Chem. Res.*, 2013, **46**, 1848–1857.

7 L. Zhang, L. T. Roling, X. Wang, M. Vara, M. F. Chi, J. Y. Liu, S. I. Choi, J. Park, J. A. Herron, Z. X. Xie, M. Mavrikakis and Y. N. Xia, *Science*, 2015, **349**, 412–416.
8 L. Z. Bu, N. Zhang, S. J. Guo, X. Zhang, J. Li, J. L. Yao, T. Wu, G. Lu, J. Y. Ma, D. Su and X. Q. Huang, *Science*, 2016, **354**, 1410–1414.
9 T. Bian, H. Zhang, Y. Y. Jiang, C. H. Jin, J. B. Wu, H. Yang and D. R. Yang, *Nano Lett.*, 2015, **15**, 7808–7815.
10 C. Chen, Y. J. Kang, Z. Y. Huo, Z. W. Zhu, W. Y. Huang, H. L. L. Xin, J. D. Snyder, D. G. Li, J. A. Herron, M. Mavrikakis, M. F. Chi, K. L. More, Y. D. Li, N. M. Markovic, G. A. Somorjai, P. D. Yang and V. R. Stamenkovic, *Science*, 2014, **343**, 1339–1343.
11 D. L. Wang, H. L. L. Xin, R. Hovden, H. S. Wang, Y. C. Yu, D. A. Muller, F. J. DiSalvo and H. D. Abruna, *Nat. Mater.*, 2013, **12**, 81–87.
12 J. B. Wu, J. L. Zhang, Z. M. Peng, S. C. Yang, F. T. Wagner and H. Yang, *J. Am. Chem. Soc.*, 2010, **132**, 4984–4985.
13 J. B. Wu, A. Gross and H. Yang, *Nano Lett.*, 2011, **11**, 798–802.
14 J. B. Wu, L. Qi, H. J. You, A. Gross, J. Li and H. Yang, *J. Am. Chem. Soc.*, 2012, **134**, 11880–11883.
15 Y. C. Yan, H. Shan, G. Li, F. Xiao, Y. Y. Jiang, Y. Y. Yan, C. H. Jin, H. Zhang, J. B. Wu and D. R. Yang, *Nano Lett.*, 2016, **16**, 7999–8004.
16 Y. L. Xiong, H. Shan, Z. N. Zhou, Y. C. Yan, W. L. Chen, Y. X. Yang, Y. F. Liu, H. Tian, J. B. Wu, H. Zhang and D. R. Yang, *Small*, 2017, **13**, 1603423.
17 Y. N. Xia, Y. J. Xiong, B. Lim and S. E. Skrabalak, *Angew. Chem., Int. Ed.*, 2009, **48**, 60–103.
18 M. Lefevre, E. Proietti, F. Jaouen and J. P. Dodelet, *Science*, 2009, **324**, 71–74.
19 E. Antolini, *Energy Environ. Sci.*, 2009, **2**, 915–931.
20 J. B. Xu, P. Gao and T. S. Zhao, *Energy Environ. Sci.*, 2012, **5**, 5333–5339.
21 H. T. Chung, J. H. Won and P. Zelenay, *Nat. Commun.*, 2013, **4**, 1922.
22 Y. Y. Liang, Y. G. Li, H. L. Wang, J. G. Zhou, J. Wang, T. Regier and H. J. Dai, *Nat. Mater.*, 2011, **10**, 780–786.
23 C. G. Hu and L. M. Dai, *Adv. Mater.*, 2017, **29**, 1604942.
24 G. Wu, K. L. More, C. M. Johnston and P. Zelenay, *Science*, 2011, **332**, 443–447.
25 J. Suntivich, H. A. Gasteiger, N. Yabuuchi, H. Nakanishi, J. B. Goodenough and Y. Shao-Horn, *Nat. Chem.*, 2011, **3**, 546–550.
26 R. Bashyam and P. Zelenay, *Nature*, 2006, **443**, 63–66.
27 L. Xiao, L. Zhuang, Y. Liu, J. T. Lu and H. D. Abruna, *J. Am. Chem. Soc.*, 2009, **131**, 602–608.
28 C. L. Lee and H. P. Chiou, *Appl. Catal., B*, 2012, **117**, 204–211.
29 C. Jeyabharathi, S. S. Kumar, G. V. M. Kiruthika and K. L. N. Phani, *Angew. Chem., Int. Ed.*, 2010, **49**, 2925–2928.
30 W. Chen and S. W. Chen, *Angew. Chem., Int. Ed.*, 2009, **48**, 4386–4389.
31 S. S. Kim, Y. R. Kim, T. D. Chung and B. H. Sohn, *Adv. Funct. Mater.*, 2014, **24**, 2764–2771.
32 B. B. Blizanac, P. N. Ross and N. M. Markovic, *J. Phys. Chem. B*, 2006, **110**, 4735–4741.

33 J. B. Wu, W. P. Gao, H. Yang and J. M. Zuo, *ACS Nano*, 2017, **11**, 1696–1703.

34 Y. Y. Jiang, G. M. Zhu, F. Lin, H. Zhang, C. H. Jin, J. Yuan, D. R. Yang and Z. Zhang, *Nano Lett.*, 2014, **14**, 3761–3765.

35 Wikipedia, Precious metal, https://en.wikipedia.org/wiki/, accessed 6, 1980.

36 W. M. Haynes, *CRC handbook of chemistry and physics*, CRC Press, Boca Raton, FL, USA, 95th edn, 2014.

37 D. J. Martin, N. Umezawa, X. W. Chen, J. H. Ye and J. W. Tang, *Energy Environ. Sci.*, 2013, **6**, 3380–3386.

38 Y. Bi, S. Ouyang, N. Umezawa, J. Cao and J. Ye, *J. Am. Chem. Soc.*, 2011, **133**, 6490–6492.

39 W. L. Xu, X. C. Zhou, C. P. Liu, W. Xing and T. H. Lu, *Electrochem. Commun.*, 2007, **9**, 1002–1006.

40 G. Wu, L. Li, J. H. Li and B. Q. Xu, *Carbon*, 2005, **43**, 2579–2587.

41 G. Che, B. B. Lakshmi, C. R. M. And and E. R. Fisher, *Langmuir*, 1999, **15**, 750–758.

42 T. Matsumoto, T. Komatsu, K. Arai, T. Yamazaki, M. Kijima, H. Shimizu, Y. Takasawa and J. Nakamura, *Chem. Commun.*, 2004, 840–841, DOI: 10.1039/b400607k.

43 W. Li, C. Liang, W. Zhou, J. Qiu, H. Li, G. Sun and Q. Xin, *Carbon*, 2004, **42**, 436–439.

44 J. B. Wu and H. Yang, *Nano Res.*, 2011, **4**, 72–82.

45 A. E. S. Sleightholme, J. R. Varcoe and A. R. Kucernak, *Electrochem. Commun.*, 2008, **10**, 151–155.

46 M. J. Simpson, A. Svendsen and P. L. Chan, *Phys. Rev. C: Nucl. Phys.*, 2007, **30**, 463–478.

47 J. Zhu, C. He, Y. Li, S. Kang and P. K. Shen, *J. Mater. Chem. A*, 2013, **1**, 14700–14705.

48 J. K. Norskov, J. Rossmeisl, A. Logadottir, L. Lindqvist, J. R. Kitchin, T. Bligaard and H. Jonsson, *J. Phys. Chem. B*, 2004, **108**, 17886–17892.